Cyber-physical data fusion in surrogate-assisted strength pareto evolutionary algorithm for PHEV energy management optimization

Li, Ji; Zhou, Quan; Williams, Huw; Xu, Hongming; Du, Changqing

DOI:
10.1109/TII.2021.3121287

License:
Other (please provide link to licence statement

Document Version
Peer reviewed version

Citation for published version (Harvard):
Li, J, Zhou, Q, Williams, H, Xu, H & Du, C 2021, 'Cyber-physical data fusion in surrogate-assisted strength pareto evolutionary algorithm for PHEV energy management optimization', *IEEE Transactions on Industrial Informatics*. https://doi.org/10.1109/TII.2021.3121287

Cyber-Physical Data Fusion in Surrogate-assisted Strength Pareto Evolutionary Algorithm for PHEV Energy Management Optimization

Ji Li, *Member, IEEE,* Quan Zhou*, Member, IEEE,* Huw Williams, Hongming Xu, and Changqing Du

***Abstract*—This paper proposes a new form of algorithm environment for multi-objective optimization of energy management system in plug-in hybrid vehicles (PHEVs). The surrogate-assisted strength Pareto evolutionary algorithm (SSPEA) is developed to optimize the power-split control parameters guided by the data from the physical PHEV and its digital twins. By introducing a 'confidence factor', the SSPEA uses the fused data of physically measured and virtually simulated vehicle performances (energy consumption and remaining battery state-of-charge) to converge the optimization process. Gaussian noisy models are adopted to emulate the real vehicle system on the hardware-in-the-loop platform for experimental evaluation. The testing results suggest that the proposed SSPEA requires less R&D costs than the model-free method that only uses the physical information, and more than 44.6% energy can be saved during the R&D process. Driven by the SSPEA, the optimized energy management system surpasses other non-DT-assisted systems by saving more than 4.8% energy.**

***Index Terms*—cyber-physical optimization; digital twin; surrogate-assisted strength Pareto evolutionary algorithm; noisy system; plug-in hybrid electric vehicle.**

I. Introduction

Electric vehicles, including battery electric vehicles (BEVs), plug-in hybrid electric vehicles (PHEVs), and fuel cell electric vehicles (FCEVs) are main contributors towards net zero emission in the transport sector [1]. To ensure the smooth entry of battery electric and other renewable vehicles into the market, hybrid and plug-in hybrid play an irreplaceable role in prior technical reserve and market expansion [2]. Energy management optimization plays an important role for them to improve the efficiency of energy utilization and improve the dynamic performance of the system, and it is a challenging task that needs to deal with many objectives, e.g., minimizing the fuel consumption and maximizing the batter life [3].

Dynamic programming [4] is a benchmark offline method to attain the global optimal control strategy of the hybrid vehicle under a given driving cycle. However, dynamic programming is not practical feasible because it cannot be directly implemented in real time control [5]. Heuristic control, including thermostat strategies [6] and state machine approaches [7], has been favored by industry for real-time energy management. As an advanced heuristic method, the state machine approach works on decentralized control of three modes, i.e., electric traction (EV) mode, charge-depleting (CD) mode, and charge-sustaining (CS) mode [8], to maximize the usage of electricity and maintain the battery's state of charge in a safe domain. But the performance is seriously affected by expert experience [9]. The equivalent consumption minimizing strategy (ECMS) [10] is an online method to transform a global minimization problem into an instantaneous minimization problem that has been solved at each time step. The equivalent factor can be evaluated on the basis of past and predicted data of the driving conditions [11]. However, the obtained driving conditions have many uncertainties caused by prediction accuracy and signal noise that will make actual performance of the vehicle system unstable. Global optimization algorithms, e.g., generic algorithm [12] and particle swarm optimization [13], have been widely applied to optimize the thresholds for mode switching with hybrid vehicle models. Since the empirical models cannot be adaptive to the real-world driving conditions, the optimization performance of using these model-based optimization schemes have been severely restricted [14]. Alternatively, non-model-based (also known as 'model-free') methods [15]–[17] are developed that allow the artificial-intelligence (AI) algorithms interact with the physical plants directly. However, such methods are costly and may include potential risks due to unnecessary trials generated by AI.

Digital twin (DT) is an emerging technology in the industry 4.0 era, which is a virtual model designed to accurately reflect a physical object. Cyber-physical data fusion is the process that integrates multiple data sources obtained by physical systems and virtual models to produce more consistent, accurate, and useful information than that provided by any individual data source [18]. It provides a cost-efficient platform for solving of high-dimensional expensive problems using artificial intelligence [19], [20]. Sensors and data transmission technologies are increasingly used to collect data throughout different stages of a PHEV's lifecycle [21]. Development of EMS for PHEV is a typical expensive problem in automotive

This work was supported in part by the State Key Laboratory of Automotive Safety and Energy under Project KF2029, in part by Jiangsu Industrial Technology Research Institute, and in part by Natural Science Foundation of China under Project 51975434. (*Corresponding author: Quan Zhou)*

Ji Li, Quan Zhou, Huw Williams, and Hongming Xu are with the Department of Mechanical Engineering, the University of Birmingham, Birmingham, B15 2TT, U.K. (e-mail: j.li.1@bham.ac.uk; g.zhou@bham.ac.uk; h.williams.5@bham.ac.uk; h.m.xu@bham.ac.uk), in which Quan Zhou and Hongming Xu are also with the State Key Laboratory of Automotive Safety and Energy, Tsinghua University, Beijing, 100084, China. Changqing Du is with the School of Automotive Engineering, Wuhan University of Technology, Wuhan, 430070, China. (e-mail: cq_du@whut.edu.cn).

industry [22]. It traditionally needs large amount the testing and verifications to guarantee the control parameters can meet the design targets [23]. DT can integrate the physical and virtual data throughout the development of EMS, which leads to a huge volume of data that can be processed by advanced analytics [24]. Then, the analysis results can be used to improve the performance of product/process in the physical space [25]. However, how to fuse the physical and virtual data for better and more robust AI-based optimization results is a big challenge for smart manufacturing.

Based on the 2nd generation strength Pareto evolutionary algorithm (SPEA-II) which incorporates a fine-grained fitness assignment strategy, a density estimation technique, and an enhanced archive truncation method, this paper proposes a surrogate-assisted SPEA (SSPEA) for DT-assisted EMS optimization. Different from the mainstream model-free and model-based schemes, the proposed SSPEA-driven optimization scheme is an interactive form of algorithm environment combining these two to reduce R&D costs and improve system robustness of PHEVs. Followed by building a digital twin of the studied PHEV, the work is conducted with four original contributions:

1) A new EMS optimization scheme is designed based on the SSPEA, where one of the computing agents interacts with the physical PHEV while the others interact with digital twins of the PHEV.
2) By introducing a 'confidence factor', which is used to calculate the weighted-sum of the measurements from the physical PHEV and its digital twins, a cyber-physical data fusion method is developed to guide the convergence of the SSPEA-based optimization process.
3) Five Gaussian noisy model are adopted to emulate the measurement noise in the real PHEV system on the Hardware-in-the-Loop (HiL) platform, which was used to comprehensively evaluate the real-time performance of the SSPEA-based control optimization system.
4) For better evaluation on DT-assisted optimization performance, two new types of evaluation criterion are introduced to quantify DT contribution in the optimization process and on-road performance.

The rest of this paper is organized as follows: the control optimization problem is formulated in Section II based on mathematical modelling of a PHEV system. Followed by digital twin modelling of the surrogate platoon, Section III introduces the SSPEA-based optimization process. Section IV sets up the noise models and the HiL platform, which are used for experimental evaluations. Section V discusses the results, and Section VI summarizes the conclusions.

II. Problem Statement

A. Vehicle Configuration

As illustrated in Fig. 1, the PHEV has a series-parallel topology, which comprises a 63kW internal combustion engine (ICE), a 32kW integrated starter-generator (ISG), and a 75kW trans-motor (i.e., an electric motor that has a float stator [26]). The main parameters for vehicle modelling are illustrated in Table I. They were sourced from the authors' recent work [27], [28] and proved by industry.

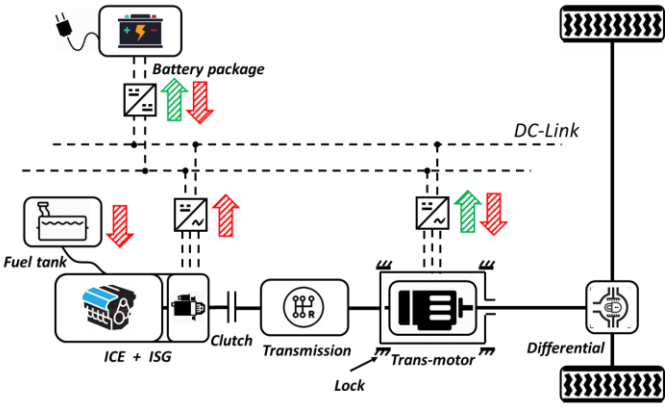

Fig. 1. The architecture of the plug-in series-parallel hybrid powertrain

By controlling the disengagement/engagement of the clutch and lock, the PHEV can work on three operational modes, i.e., EV mode, parallel mode, and series mode. If the clutch is disengaged, and Lock is engaged, the PHEV will work at the EV mode like an electric vehicle. If the clutch is engaged, and Lock is disengaged, the PHEV will work at the parallel mode where the engine is used for propulsion. If the clutch is disengaged, and lock is engaged, the PHEV will work at the series mode where the engine is used for charging the battery.

TABLE I
MAIN PARAMETERS OF THE VEHICLE MODEL

Symbol	Parameters	Values
m	Gross mass	$1{,}500kg$
A_f	Windward area	$2m^2$
R_{wh}	Tire rolling radius	$0.3m$
C_d	Air drag coefficient	0.3
i_0	Differential ratio	3.75
i_g	Transmission ratio	3.55/1.96/1.30/0.89/0.71
η_{i0}	Differential efficiency	0.95

A backward facing vehicle model considering longitudinal dynamics is used in this study. The torque demand T_d and rotation speed demand n_d after a bi-level-gear speed reducer are:

$$\left.\begin{aligned} T_d &= \left(\delta ma + \frac{C_d A_f u^2}{21.15} + mgsin\theta + mgfcos\theta\right)\cdot\frac{R_{wh}}{i_0\cdot\eta_{i0}} \\ n_d &= 9.55\cdot\frac{u}{3.6\cdot R_{wh}} \end{aligned}\right\} \quad (1)$$

where, $g = 9.81m/s^2$ is gravitational constant; $\delta = 1$ is the coefficient of rolling friction; u is the vehicle speed in km/h which is defined by driving cycles; $\theta = 0$ is slope grade; 9.55 is a conversion coefficient from radian per second to revolution per minute.

Since the powers from two powerplants are coupled together by coupling their speeds, the characteristics of a speed coupling can be described by

$$\left.\begin{aligned} n_d &= n_{mot} + n'_{ice} \\ T_d &= T_{mot} = T'_{ice} \end{aligned}\right\} \quad (2)$$

where n_{mot} and T_{mot} are speed demand and torque demand of the traction motor, respectively; n'_{ice} and T'_{ice} are speed demand and torque demand of the ICE after transmission, respectively. Finally, the speed demand and toque demand of the ICE can be calculated via transmission ratio:

$$\left.\begin{aligned} n_{ice} &= n'_{ice}\cdot i_g \\ T_{ice} &= T'_{ice}\cdot i_g \end{aligned}\right\} \quad (3)$$

where n_{ice} and T_{ice} are the speed demand and toque demand of the ICE, respectively. For this model to be valid, we assume the PHEV has an available energy budget for a particular journey.

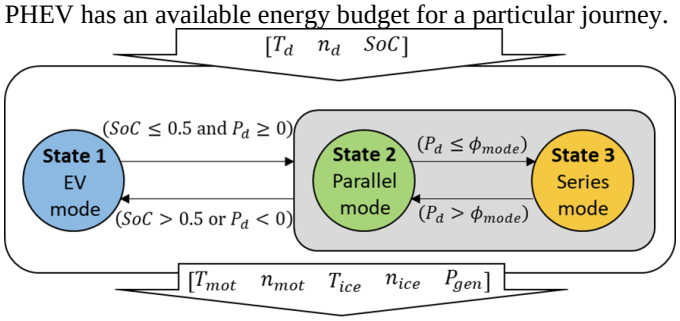

Fig. 2. State machine for energy management of the PHEV

B. Energy Management Strategy

A typical state machine [29], as shown in Fig.2, is adopted in this paper to control the transition between three operation modes. This control strategy is highly appropriated for energy management of PHEVs.

The inequalities in Fig.2 illustrates the conditions that are used to switch the operation modes, and in each mode, the PHEV implements different power split strategies to satisfy the power demand for vehicle operation. The state machine controller has three inputs: vehicle torque demand, T_d, speed demand, n_d, and battery state of charge, SoC. The output of the state machine is a power-split vector:

$$\boldsymbol{\xi} = [T_{mot} \quad n_{mot} \quad T'_{ice} \quad n'_{ice} \quad P_{gen}] \tag{4}$$

where T_{mot} and n_{mot} are the torque demand and speed demand of the trans-motor, respectively; and P_{gen} is the power demand of the ISG.

In the EV mode (when $SoC > 0.5$ or $P_d < 0$), the PHEV will work like a battery electric vehicle, therefore, the power-split vector under the EV mode is:

$$\boldsymbol{\xi} = [T_d \quad n_d \quad 0 \quad 0 \quad 0] \tag{5}$$

In the series and parallel modes (when $SoC \leq 0.5$ and $P_d \geq 0$), switching between series and parallel modes are governed by the power demand, P_d, and a control parameter, ϕ_{mode}. If $P_d > \phi_{mode}$, the vehicle will work on parallel mode otherwise the vehicle will work on series mode. The power-split vector for series mode and parallel mode are:

$$\boldsymbol{\xi} = \begin{cases} [T_d \quad n_d \cdot (1-\chi_1) \quad T_d \quad n_d \cdot \chi_1 \quad 0] & Series \\ [T_d \quad n_d \quad T'_{ice}(P_{gen}) \quad n'_{ice}(P_{gen}) \quad P_{gen^+} \cdot \chi_2] & Parallel \end{cases} \tag{6}$$

where, T'_{ice} and n'_{ice} are optimal torque and speed of the ICE converted based on demand power of the ISG, P_{gen}; P_{gen^+} is the peak power of the ISG; and χ_i (i =1 or 2) is a proportionality factor determined by

$$\chi_i(SoC) = \begin{cases} 1, & SoC \in [0,0.2] \\ \left\{1 + \exp\left[\left(\frac{SoC}{SoC^*} + \phi_{i,\beta}\right)\phi_{i,\alpha}\right]\right\}^{-1}, & SoC \in (0.2,0.5] \\ 0, & SoC \in (0.5,1] \end{cases} \tag{7}$$

where, SoC^* is a scaling coefficient of the battery's SoC; $\phi_{i,\alpha}$ (i=1 or 2) $\in [0.01,50]$ and $\phi_{i,\beta}$ (i=1 or 2) $\in [-6,6]$ are four control parameters for ICE and ISG; and χ_1 and χ_2 are for ICE control and ISG control, respectively [30].

C. Optimization Problem Formulation

This paper studied a bi-objective optimization problem in PHEV energy management. The first optimization objective is to minimize the total energy consumption in fuel and electricity, J_1.

The equivalent power of fuel consumption, P_{fuel}, can be determined by

$$P_{fuel} = 3.6 \times 10^6 Q_{LHV} \cdot BSFC(T_{ice}, n_{ice}) \tag{8}$$

where Q_{LHV} is the lower heating value in kJ/kg and BSFC is the brake specific fuel consumption in g/kWh.

The power consumption in the battery, P_{bp}, can be calculated by:

$$P_{bp} = T_{mot} \cdot n_{mot} - P_{gen} \tag{9}$$

The second optimization objective is to maximize value of the remaining battery's SoC at end of a given driving cycle, J_2, as considered in [28]. The battery SoC can be calculated by:

$$SoC = SoC_0 - \int_0^t \frac{I}{Q_{bc}} dt \tag{10}$$

where SoC_0 is the initial BP's SoC; Q_{bc} is the battery cell charge capacity; and I is the battery cell current, which can be calculated by

$$I = \frac{P_{bp}}{n_{bc} \cdot V_{bc}(SoC)} \tag{11}$$

where, n_{bc} is the number of the battery's cells; $V_{bc}(SoC)$ is battery terminal voltage expressed as a function of the SoC. The battery cell data and calibrated model parameters are supplied by Panasonic Automotive & Industrial System Ltd.

Consequently, the two objectives can be formulated as:

$$\left.\begin{aligned} J_1 &= \int_0^t \left(P_{fuel} + P_{bp}\right) dt \\ J_2 &= \frac{1}{SoC_{end}} \end{aligned}\right\} \tag{12}$$

where, SoC_{end} is the value of remaining battery's SoC at the end of a given driving cycle.

The optimization objectives will be achieved by retrieving the optimal combination of the control parameters i.e., $\phi^*_{1,\alpha}$, $\phi^*_{1,\beta}$, $\phi^*_{2,\alpha}$, $\phi^*_{2,\beta}$, and ϕ^*_{mode} (as in Fig. 2). Finally, the optimization problem of control parameters is described by

$$\begin{aligned} \left[\phi^*_{1,\alpha} \quad \phi^*_{1,\beta} \quad \phi^*_{2,\alpha} \quad \phi^*_{2,\beta} \quad \phi^*_{mode}\right] &= \arg\min(J_1 \quad J_2) \\ s.t. \begin{cases} SoC \in [0.2,0.8] \\ n_{mot} \in [0, n_{mot^+}] \\ T_{mot} \in [T_{mot^-}, T_{mot^+}] \\ P_{ice} \in [0, P_{ice^+}] \\ P_{gen} \in [0, P_{gen^+}] \end{cases} \end{aligned} \tag{13}$$

where the state of charge must be maintained between 0.2 and 0.8 for safe and efficient use; n_{mot^+} is the maximum speed of the traction motor; T_{mot^-} and T_{mot^+} are minimum and maximum torque of the traction motor, respectively. P_{ice^+} is the maximum power of the ICE; and P_{gen^+} is the maximum power of the ISG. All power machines should operate in their own working ranges.

III. Proposed Solution

The mainstream control optimization schemes include model-free scheme (algorithm interacts directly with the real

vehicle system (RVS)) and model-based scheme (algorithm interacts purely with an empirical model). The former uses heavy experimental effort in exchange for better system performance. The latter requires expert experience on empirical model development. The proposed SSPEA-driven optimization scheme, as illustrated in Fig.3, is an interactive form of algorithm environment combining model-free scheme and model-based scheme.

It includes two main procedures: 1) firstly a neuro-fuzzy digital surrogate platoon is built to encapsulate the real vehicle system (RVS) that involves a theorical vehicle model and a Gaussian noise model; and 2) a surrogate-assisted strength Pareto evolutionary algorithm (SSPEA) is developed for a mixed cyber-physical environment that includes the digital surrogates and physical measurement. Detailed development procedures of these two developments are introduced in the following sections.

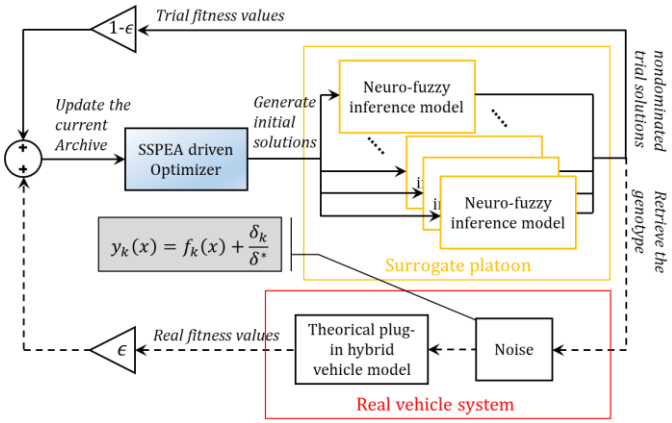

Fig. 3. Schematic diagram of the SSPEA-driven optimization scheme

A. Neuro-Fuzzy Modelling of Surrogate Platoon

The surrogate platoon is built based on an adaptive neuro-fuzzy inference system (ANFIS) model because ANFIS can construct any nonlinear mapping with prior knowledge in fuzzy rules and have the model parameters auto-calibrated in a way like artificial neural networks [31]. Fig. 4 displays the flowchart of neuro-fuzzy modelling process consisting of two main stages of data preprocessing and model establishment as considered in [32].

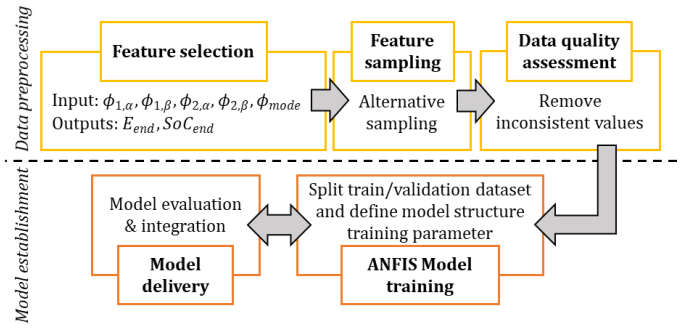

Fig. 4. Flowchart of neuro-fuzzy modelling process

In data preprocessing, firstly, features of inputs and outputs are defined as shown in Fig. 4. To ensure the diversity of samples, an alternative sampling method is then adopted to capture features of inputs and outputs. Before the ANFIS model establishment, data quality assessment should be carried out to remove inconsistent values caused by system noise. In model establishment, the ANFIS is based on a first order Sugeno model that compromises several rule sets, where one of the rule sets can be expressed as

Rules *i*:

$$\text{If } (x \text{ is } A_i) \text{ and } (y \text{ is } B_i) \text{ then } (f_i = \alpha_i x + \beta_i y + \gamma_i) \quad (14)$$

where x and y are the inputs; A_i and B_i are the fuzzy sets determined during the network training procedure; f_i is output, α_i, β_i, and γ_i are linear parameters, which will be determined in model learning. In this paper, the input-output relation of one ANFIS model can be expressed as follows:

$$[E_{end}, SoC_{end}] = \Gamma_{NF}(\phi_{1,\alpha}, \phi_{1,\beta}, \phi_{2,\alpha}, \phi_{1,\beta}, \phi_{mode}) \quad (15)$$

where, Γ_{NF} is a ANFIS model of five inputs and two outputs; $\phi_{1,\alpha}, \phi_{1,\beta}, \phi_{1,\alpha}, \phi_{1,\beta}, \phi_{mode}$ denote the five control parameters jointly define the position and slope of the curve in the logistic function and the threshold of mode transition; and E_{end} and SoC_{end} denote two outputs of the total energy consumption and the remaining SoC's value, respectively. After model evolution, the trained ANFIS model will be used as digital surrogate platoon for energy management optimization.

B. Surrogate-assisted Strength Pareto Evolutionary Algorithm

The surrogate-assisted strength Pareto evolutionary algorithm (SSPEA), Fig. 5, is proposed by adding hybrid data interfaces and a 'confidence factor' to a standard SPEA-II, where the data interfaces allow the SSPEA to interact with the RVS and the neuro-fuzzy surrogate platoon. So that the PHEV control parameters can be effectively optimized via two type feedbacks from the data interfaces. The specific steps of the SSPEA are described as follows:

1) **Initialization:** With the generation counter, t ($t = 0,1,\dots,T$), initialized as zero, a group of the control parameter sets $\phi_{1,\alpha}$, $\phi_{1,\beta}$, $\phi_{2,\alpha}$, $\phi_{2,\beta}$, ϕ_{mode}.

2) **Trial fitness acquisition:** As marked in blue, the trial fitness values of the two objectives, J_1 and J_2, are obtained from parallel simulation of the surrogate platoon with different control parameters provided by the individuals in population P_t and external archive A_t. A strength value, $S(i)$, is assigned for individual i ($i = 1,2,\dots,N$), which indicates the number of solutions that can be dominated by the individual in P_t and A_t. The raw fitness value, $R(i)$, is calculated as the sum of the strength values, $S(i)$. To distinguish the individuals sharing the same raw fitness value, the density information, σ_i^k, is introduced which indicates the space distance between the individual i and the kth nearby individual. The kth nearest neighbor method is adopted to calculate the density value $D(i)$ of individual i [33], i.e., $D(i) = \frac{1}{\sigma_i^k + 2}$. Finally, the fitness value of individual i, $F(i)$, is the sum of the raw fitness value, $R(i)$, and the density value, $D(i)$.

3) **Fitness assignment:** All trial nondominated individuals, i.e., the current best control parameter sets in P_t and A_t are copied to A_{t+1}. If the size of A_{t+1} is larger than $\overline{N}$ (archive size), then reduce A_{t+1} by means of the truncation operator;

else, fill $A_{t+1}$by the dominated individuals in P_t and A_t until the size equals to N (the population size).

4) **Fitness correction:** As marked in red, the real fitness values $F^*(i)$ of individual i in archive A_{t+1} are validated by calling the RVS in series. A 'confidence factor' $\epsilon \in [0,1]$ is introduced to regulate the fitness values of all individuals in A_{t+1} by

$$F(i) = (1-\epsilon)\cdot S(i) + \epsilon \cdot F^*(i) \qquad (16)$$

where, F^* is the validation results; and S is the simulation results obtained with the surrogate platoon.

5) **Environmental Selection, Evolutionary Operations, and Termination:** The rest of procedures follow the setting of the standard SPEA-II. Environmental selection is conducted based on the size of A_{t+1}, if the size of A_{t+1} is larger than the archive size, $\overline{N}$, then A_{t+1} is reduced by a truncation operator; otherwise, A_{t+1} is filled by the dominated individuals in P_t and A_t until the size equals to $\overline{N}$. Termination condition is set based on the generation counter value, t. If $t \geq T$, the nondominated set A_t is copied to A_{t+1} and terminate the optimization; otherwise, evolutionary operations including crossover and mutation are implemented to the mating pool, and the generation counter is set to $t+1$. To fill the mating pool, a binary tournament selection is applied to update A_{t+1}; then, the procedures from Step 2-5 are repeated until the termination condition is met.

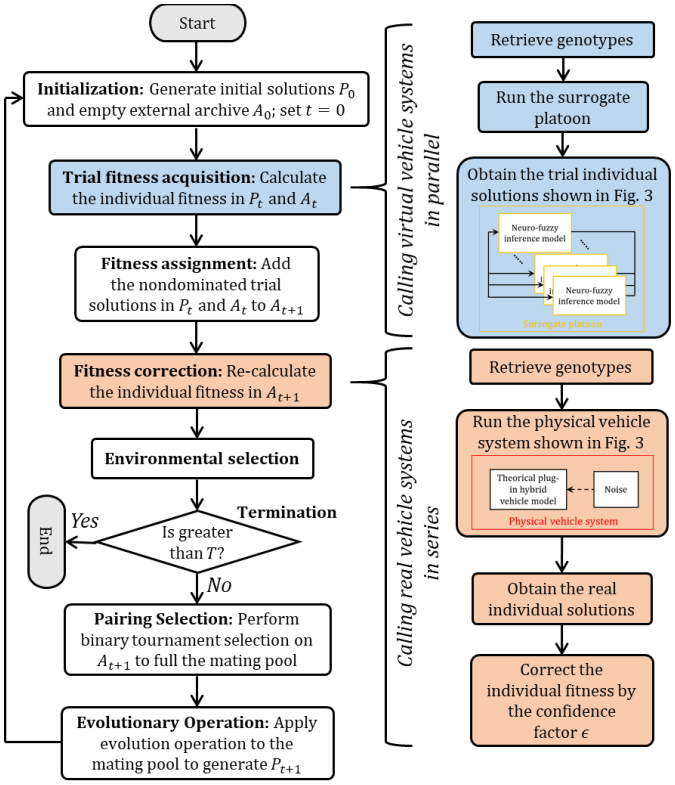

Fig. 5. Flowchart of surrogate-assisted strength Pareto evolutionary algorithm

IV. Testing and Validation Set-up

A. Noise Models

To emulate the measurement noises in the RVS, the objective functions are contaminated with noise samples taken from the representative Gaussian distributions. Mathematically, the noisy level of the kth objective function with a trial solution x is defined by [34]

$$y_k(x) = f_k(x) + \frac{\delta_k}{\delta^*}, \qquad \delta \sim N(\mu, \sigma^2) \qquad (17)$$

where δ_k represents the stochastic noise amplitude that follows a certain probability distribution function; δ^* is a scaling factor that normalize the effect of δ_k on $f_k(x)$.

Gaussian functions with the five typical probability distributions are applied to represent the mean values and variances of the measurement errors, i.e., Gau-I ($\mu = 0, \sigma^2 = 0.2$), Gau-II ($\mu = 0, \sigma^2 = 0.5$), Gau-III ($\mu = 0, \sigma^2 = 1$), Gau-IV ($\mu = 0, \sigma^2 = 5$), and Gau-V ($\mu = -2, \sigma^2 = 0.5$).

B. Hardware-in-the-Loop Facilities

Hardware-in-the-loop (HiL) testing is conducted to evaluate the real-time performance of the cyber-physical system, which uses industrial level real-time testing facilities provided by the ETAS Group. The HiL system is set-up as in Fig. 6.

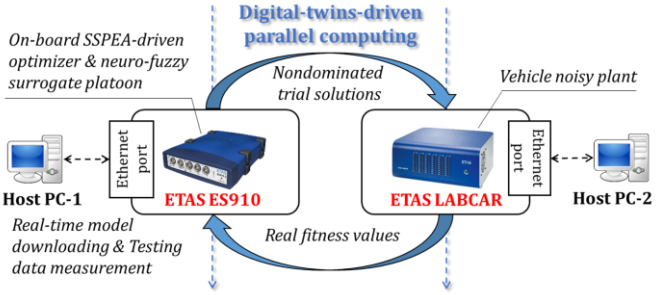

Fig. 6. Hardware-in-the-loop testing bench

The energy management optimization is jointly performed by an ETAS ES910 and an ETAS LABCAR. The ES910 includes a 1.5GHz microprocessor with 4GB RAM and 1Gbps Ethernet communication. The surrogate platoon and SSPEA-driven optimizer are established and compiled in host PC-1 and flashed to the ES910 via ETAS INTECRIO. The vehicle noisy plant regarded as an RVS is programmed into host PC-2 and downloaded to LABCAR by the ETAS experimental environment via Ethernet protocol. In this study, the sampling frequency of the system is 10 Hz and of the band-limited white Gaussian noise is 4 Hz (due to Nyquist Sampling Theorem). The vehicle performance is supervised by the ETAS experimental environment in host PC-2.

V. Results and Discussion

A. Surrogate Learning Performance

To guarantee the digital surrogate can accurately predict the powertrain performance with different control settings, the surrogate models obtained by different learning methods and data topologies are evaluated and compared. The learning space is generated through data sampling in linear spaces. In terms of learning methods, a hybrid algorithm, which incorporates the least square estimation to the backpropagation (BP) method to accelerate the convergence, is adopted and compared to the conventional BP method. Three different training data topologies are investigated, where each input of the digital surrogate has three sampling sizes of 3, 5, and 7, respectively. The training results are obtained from the noisy vehicle systems

by running the model learning algorithm for 30 runs individually.

Fig. 7 illustrates statistical results in surrogate training, where training time (TT) and root mean square error (RMSE) of using conventional BP and the hybrid algorithm are compared. The hybrid algorithm is better than the conventional BP algorithm because the results obtained by the hybrid algorithm achieves lower variance and mean of RMSE than that obtained by the conventional BP algorithm. In conjunction with the impact of dataset split ratio on testing performance as shown in Fig. 8, as an increase of the dataset split ratio for training, RMSEs obtained by both algorithms decrease rapidly first and then go stable gradually. Considering this, 80% random samples of dataset are for training while the rest is used for testing.

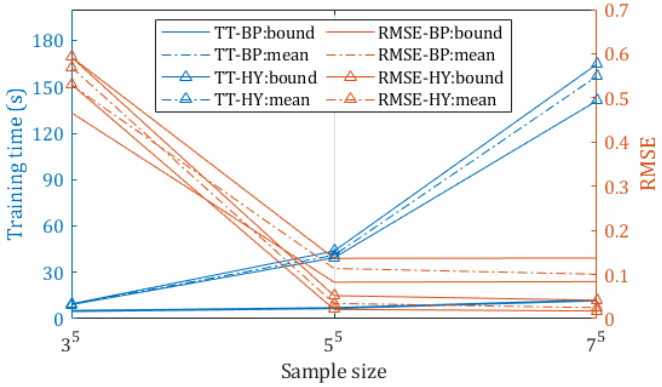

Fig. 7. Statistical results of training performance of surrogate platoon at different data topologies

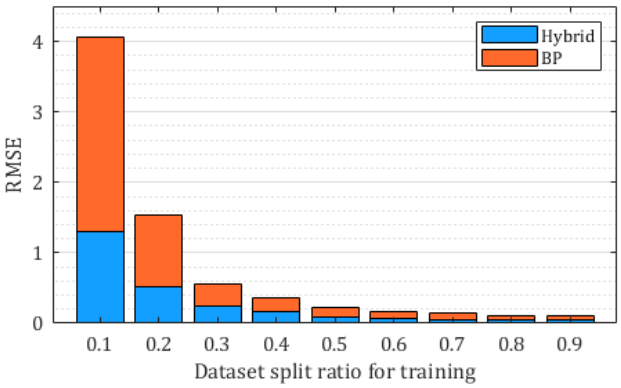

Fig. 8. Impact of dataset split ratio on testing performance

Detailed comparations of the model learning methods with different noisy systems are presented in Table II. The 5^5 data topology shows that is applicable in surrogate learning, which can significantly reduce the testing RMSE by at least 80% compared to 3^5 data topology. It also helps save more than 413% (115s) training time compared to 7^5 data topology while achieving similar training performance. Since 5^5 data topology already provides enough training samples to describe a high-fidelity surrogate platoon, a surrogate platoon trained by hybrid algorithm with 5^5 data topology will be applied in the SPPEA.

B. *Impact of Using Different Confidence Factors*

This section discusses the effectiveness of the proposed SSPEA with different 'confidence factor' values, i.e., $\epsilon = 0, 0.25, 0.5, 0.75,$ and 1. Both Pareto performance and number of RVS calls will be monitored to evaluate the optimization performance and computational efforts. Control optimization with other two mainstream optimization schemes, i.e. model-free scheme (SPEA-II algorithm interacts directly with the RVS) and model-based scheme (SPEA-II algorithm interacts purely with an empirical model [35]), are investigated as the baseline. For a fair comparison, all optimization schemes have same population size, i.e., $N = 50$, same archive size, i.e., $\overline{N} = 50$, same probability of crossover and mutation rates, i.e., $p_{cro} = 0.7$ and $p_{mut} = 0.3$, and same termination criterion, i.e., no more than 100 iterations. Here, generational distance (GD) is used to evaluate estimated Pareto frontiers (ePF) obtained by the studied optimization schemes: if an optimization scheme can achieve the smaller GD value than the others the scheme is better than the others. GD is calculated by [36]:

$$\mathrm{GD} = \frac{\sqrt{\sum_{m=1}^{M} y_m \cdot \mathrm{dis}^2(y_m, \boldsymbol{S}_{\mathrm{aPF}})}}{N} \tag{18}$$

where M is the member of elements in the ePF; y_m is the individual value in the ePF sets; $\boldsymbol{S}_{\mathrm{aPF}}$ is a set that forms the approximated Pareto frontier (aPF); $\mathrm{dis}(y_m, \boldsymbol{S}_{\mathrm{aPF}})$ is the shortest distance between the element y_m and the aPF.

As illustrated in Fig. 9, there are estimated Pareto frontiers (ePF) obtained with the studied methods and an approximated Pareto frontier (aPF), which is obtained by calculating the nondominated set from all the ePF. As the results, the solutions

TABLE II
SURROGATE TRAINING PERFORMANCE COMPARISON

Conditions		Training time (s)		Training error (RMSE)		Testing error (RMSE)		Training efficiency (ΔRMSE/s)	
Noise type	Sample size	BP	Hybrid	BP	Hybrid	BP	Hybrid	BP	Hybrid
Gau-I	3^5	4.87	9.13	0.1188	0.0000	0.4686	0.5686	-	-
	5^5	6.55	40.20	0.0882	0.0072	0.1098	0.0523	-0.2136	-0.0166
	7^5	11.93	140.93	0.1000	0.0182	0.1005	0.0211	-0.0521	-0.0042
Gau-II	3^5	4.88	9.60	0.1256	0.0000	0.5922	0.5922	-	-
	5^5	6.95	39.44	0.9812	0.0070	0.0828	0.0386	-0.2461	-0.0186
	7^5	12.17	164.38	0.0941	0.0198	0.0840	0.0235	-0.0697	-0.0037
Gau-III	3^5	4.67	9.27	0.1053	0.0000	0.5308	0.5308	-	-
	5^5	6.78	41.30	0.0959	0.0094	0.1367	0.0211	-0.1868	-0.0159
	7^5	11.57	158.38	0.0810	0.1392	0.0866	0.0175	-0.0644	-0.0034
Gau-IV	3^5	5.36	9.56	0.1059	0.0000	0.5883	0.5883	-	-
	5^5	7.18	43.80	0.0958	0.0091	0.1291	0.0270	-0.2523	-0.0164
	7^5	11.65	155.74	0.1228	0.0378	0.1373	0.0418	-0.0717	-0.0037
Gau-V	3^5	4.82	9.11	0.0624	0.0000	0.4664	0.5664	-	-
	5^5	6.65	40.69	0.1037	0.0095	0.1106	0.0341	-0.1944	-0.0169
	7^5	12.04	164.64	0.0910	0.0172	0.0956	0.0210	-0.0514	-0.0035

of using model-based or SSPEA-driven optimization with $\epsilon = 0$ schemes are hard to form ePFs. Fig. 10 presents the number of RVS calls and the GD of both the proposed and baseline methods. Generally, the GD can be reduced by increasing the number of RVS calls. The SSPEA-driven scheme with $\epsilon = 0.25$ has excellent optimality, in which the GD is reduced by 69.8% compared to the model-based one. By increasing the 'confidence factor' value, number of calling the RVS increases, ending at 4144. Although the result of using the model-free optimization topology performs the shortest GD in the studied event, 1.0% improvement on the GD with sacrifice of up to 59.4% increase in the number of RVS calls is not cost efficient. Therefore, the proposed optimization scheme with $\epsilon = 0.25$ is the most thoughtful way to balance the tradeoff between the number of the calls and GD.

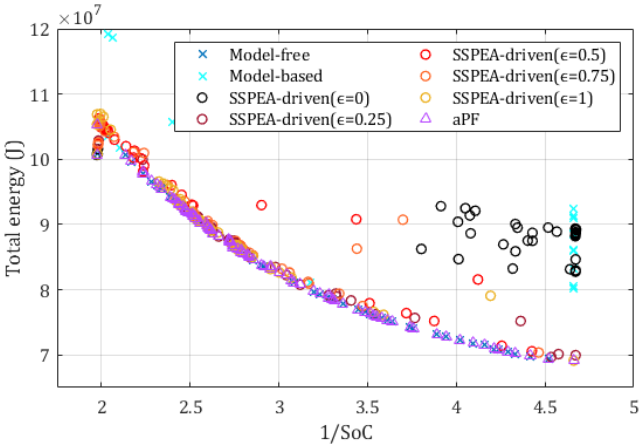

Fig. 9. Pareto frontier comparison of using three optimization schemes

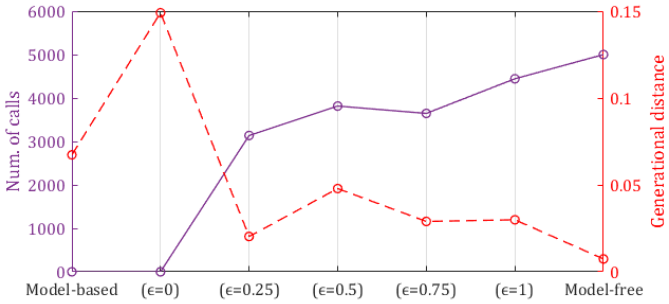

Fig. 10. Relationship between the number of real vehicle system calls and the GD

C. Optimization Performance and Computational Costs

To testify the robustness and convergence of the studied optimization scheme, 15 groups of testing are conducted under five different noisy conditions with the optimization scheme and two baseline schemes, i.e., the model-free scheme and the model-based scheme. With 30 individual tests repeated for each group, the mean and standard derivation (SD) of the GD values are computed.

In Table III, the values of mean and SD obtained by the SSPEA-driven scheme are very close to the results obtained by model-free one that can be recognized as the grand truth. Because the SSPEA-driven scheme can be adapted to the real system by involving the real measurements with digital twin, it achieved much better optimization results (lower mean and SD of the GD values) than the model-based scheme. Besides, the number of RVS calls and energy used in optimization of the three methods under the five conditions are also investigated. Compared to the model-free scheme, the SSPEA-driven scheme saves up to 44.6% energy in the optimization processes because of a significant reduction on the RVS calls. Therefore, the SSPEA-driven scheme is shown more cost-benefit than other two baseline methods.

TABLE III
OPTIMIZATION PERFORMANCES AND COMPUTATIONAL COSTS

Noise type	Optimization scheme	GD		Num. of RVS calls	Energy used in R&D (10^{11}J)
		Mean (10^{-3})	SD (10^{-4})		
Gau-I	Model-free	7.266	6.224	5000	5.272
	Model-based	87.21	48.44	0	0
	SSPEA-driven	9.518	6.212	2830	3.011
Gau-II	Model-free	13.14	15.00	5000	5.288
	Model-based	87.89	56.36	0	0
	SSPEA-driven	16.67	9.392	2766	2.932
Gau-III	Model-free	8.013	10.89	5000	5.404
	Model-based	68.47	44.75	0	0
	SSPEA-driven	20.13	9.189	3137	3.337
Gau-IV	Model-free	24.59	29.17	5000	5.765
	Model-based	143.3	74.51	0	0
	SSPEA-driven	27.09	14.53	3921	4.235
Gau-V	Model-free	18.86	20.32	5000	5.572
	Model-based	372.6	229.7	0	0
	SSPEA-driven	29.41	15.75	3025	3.277

D. Control System Adaptability

This section further evaluates the adaptability of the PHEV control system using the SSPEA-driven scheme with the SSPEA. A set of the optimal control parameters for the studied PHEV are obtained by the proposed scheme under the Gau-II condition. To determine a specific solution used in this case, a desirability function approach as applied in [37] is adopted to search one desirable solution from the ePF based on decision makers. The result of optimal control parameters from the desirable solution is listed in Table IV.

TABLE IV
OPTIMIZED RESULT OF THE CONTROL PARAMETERS

Parameter	$\phi_{ice,\alpha}$	$\phi_{ice,\beta}$	$\phi_{gen,\alpha}$	$\phi_{gen,\alpha}$	ϕ_{mode}
Value	0.010	0.282	0.384	0.024	66400

With the parameters in Table IV, the improved PHEV state-machine-based strategy (i.e., SSPEA-SM) is compared to two commonly used control strategies, i.e., the equivalent consumption minimizing strategy (ECMS) [10] and the state-machine-based strategy that is optimized by the model-based scheme using the standard SPEA-II [38] (i.e., SPEA-II-SM). The comparison study is conducted in the real-time HiL platform by running the Worldwide Harmonized Light Vehicle Test Cycle (WLTC) repeatedly for two rounds with an initial battery SoC of 50%. This is to keep the vehicle operating in series and parallel modes for exposing the advantages of using the proposed algorithm. To evaluate the vehicle system robustness, noise scenario is introduced that is the emulated signal noise in the real measurement during real-world driving. Five noise scenarios with the student's t distribution, Rayleigh distribution, Exponential distribution, and Random distribution are studied, in which these distributions are used to generate random variables and then respectively overlay on input signals. The results are obtained in Table V, wherein the reduction shows energy saves from the vehicle system by using ECMS.

Under the ideal non-noise scenario, ECMS performs a better energy economy compared to SPEA-II-SM and SSPEA-SM control strategies Between SPEA-II-SM and SSPEA-SM strategies, a discrepancy between the theoretical model and its DT results in further amplified energy consumption. In other five studied noise scenarios, the control system optimized by the SSPEA-driven scheme has strong adaptability because it allows genotypes converge to the ground truth by regulating the fitness value with both real measurement and DT-based simulation. It surpasses the benchmark methods by up to 13.81% than ECMS and up to 5.59% than the SPEA-II-SM strategy. The ECMS is able to interact with the RVS to reduce equivalent fuel consumption in real time, however two objectives of the final value of SoC and energy consumption are not satisfactory. Due to system noises, the observed state with errors will affect the instantaneous evaluation. SPEA-II-SM strategy uses global evaluation during optimization process and saves up to 8.66% energy consumption compared to the ECMS. Nevertheless, the solutions obtained by the model-based scheme (with the SPEA-II) cannot entirely fit to the RVS due to no consideration on the noise factors. In addition, the control system using SSPEA-SM strategy has similar energy-saving performance in Gaussian and Student's t noise scenarios, because Student's t-distribution [39] is like the Gaussian distribution with its bell shape but has heavier tails. It has a greater chance for extreme values than normal distributions, hence the fatter tails.

TABLE V
CONTROL PERFORMANCE UNDER DIFFERENT NOISE SCENARIOS

Noise scenario	Control strategy	Final SoC	Energy consumption (10^8J)	Reduction (%)
None	ECMS	0.266	1.002	-
	SPEA-II-SM	0.332	1.039	-3.74%
	SSPEA- SM	0.335	1.047	-4.50%
Gaussian	ECMS	0.243	1.128	-
	SPEA-II-SM	0.344	1.113	1.33%
	SSPEA-SM	0.468	1.074	4.79%
Student's t	ECMS	0.236	1.144	-
	SPEA-II-SM	0.421	1.097	4.20%
	SSPEA-SM	0.467	1.080	5.59%
Rayleigh	ECMS	0.261	1.228	-
	SPEA-II-SM	0.397	1.141	7.32%
	SSPEA-SM	0.464	1.081	11.97%
Exponential	ECMS	0.260	1.174	-
	SPEA-II-SM	0.427	1.130	3.42%
	SSPEA-SM	0.462	1.087	7.52%
Random	ECMS	0.252	1.274	-
	SPEA-II-SM	0.402	1.163	8.66%
	SSPEA-SM	0.458	1.098	13.81%

Note: The equivalent factor used in ECMS is set to $s_{opt} = 2.94$ as considered in [40].

E. Evaluation Criteria for DT-assisted Optimization

DT-assisted optimization is a new concept for PHEV EMSs where one of the computing agents interacts with the physical PHEV while the others interact with digital twins of the PHEV. For better evaluation on DT-assisted optimization performance, two new types of evaluation criterion are introduced to quantify DT contribution in the optimization process and on-road performance. The first criterion is a factor of interactive conversion, which is defined as follows.

$$C_{1.1} = E_{real} \cdot n_{call} \quad (19a)$$

$$C_{1.2} = E_{real} \cdot E_{R\&D} \quad (19b)$$

where, E_{real} is energy consumption of the PHEV system under real (noise) driving scenarios when using the same optimization scheme; n_{call} is the corresponding number of RVS calls; and $E_{R\&D}$ is energy used in R&D process. These two versions of the first criterion are used to reflect the benefit of interactive conversion during experiment and on-road testing, which is the lower the better. The main difference of these two is that n_{call} is more suitable for higher communication cost cases (e.g., Cloud-based optimization) and $E_{R\&D}$ is more suitable for higher operation cost in each interaction (e.g., EMS optimization).

The second criterion is a noise cost coefficient, which is defined as follows.

$$C_2 = \frac{E_{real}}{E_{ideal}} \quad (20)$$

where, E_{real} and E_{ideal} are energy consumption of the PHEV system under real (noise) and non-noise scenarios when using the same optimization scheme. The second criterion is used to reflect how much gain of energy consumption to various noise scenarios. The high value of the noise cost coefficient means the more distorted the model used in DT-assisted optimization.

TABLE VI
RESULTS OF NEW CRITERIA FOR THREE OPTIMIZATION SCHEMES

New criteria	Model-based	SSPEA-driven	Model-free
Interactive conversion factor	NA	3.641×10^{19}J^2	6.495×10^{19}J^2
Noise cost coefficient	1.086	1.036	1.047

Table VI shows these two criterion results for the studied case. Since the experiment cost is mainly from high-frequency operation, Eq. (19a) is adopted here to evaluate their overall benefit of experiment cost and optimization results. Due to no interaction in model-based optimization, the equivalent interaction cost is not applicable for this scheme. Compared to Model-free one, SSPEA-driven scheme helps to reduce the equivalent interaction cost by 43.9%. Regarding noise cost coefficient, the SSPEA-driven scheme can obtain the lowest value of noise cost coefficient in the studied three. It means the EMS optimized by the SSPEA-driven optimization scheme has stronger robustness for various noise scenarios. Through comprehensive study, finally, the overall performance of three optimization schemes is qualitatively summarized in Table VII. The proposed SSPEA-driven optimization scheme demonstrates its overall performance superior to other two.

TABLE VII
OVERALL EVALUATION SUMMARY OF THREE OPTIMIZATION SCHEMES

Overall criteria	Model-based	SSPEA-driven	Model-free
Expertise requirement	High	Low	Low
Experimental effort	Low	Moderate	High
On-road performance	Low	High	High
Interactive conversion factor	NA	High	Low
Noise cost coefficient	High	Low	Moderate

In summary, the proposed scheme has a capability to improve on-road performance of PHEV systems with low

expertise requirement. It also has a great potential to be applied for other industrial cases such as production and manufacturing optimization. To ensure successfully implement the proposed algorithm for optimizing these complex nonlinear systems, sampling and feature selection methods should be carefully considered to guarantee the accuracy of the DT model used for an interactive form of algorithm environment.

VI. Conclusions

This paper proposed a new form of algorithm environment for multi-objective optimization of energy management system in plug-in hybrid vehicle (PHEVs). The strength Pareto evolutionary algorithm (SSPEA) using fused cyber-physical information is developed to optimize the power-split control parameters of PHEVs. Through the HiL testing, this cyber-physical data fusion technology is comprehensively evaluated in terms of surrogate learning performance, impact of using different confidence factors, optimization performance, computational efforts, and the control system adaptability when working in different noise scenarios. The conclusions drawn from the investigation are as follows:

1) The hybrid algorithm consisting of backpropagation and least squares estimation for the DT-based surrogate platoon modelling outperforms the conventional backpropagation algorithm in model learning by achieving 75.2% less RMSE.
2) Compared to the model-based scheme, the SSPEA-driven scheme has better multi-objective optimization capability because it can significantly lessen the generational distance by up to 69.8%.
3) The SSPEA-driven scheme has achieved comparable performance as the model-free one but with 44.6% less energy used by the real vehicle system in optimization process.
4) In the robustness test, the optimized system has strong adaptability that its overall energy-saving performance surpasses other non-DT-assisted systems optimized by using ECMS (by up to 13.8%) and SPEA-II (by up to 5.6%).

References

[1] Y. Zhou, A. Ravey, and M. Péra, "A survey on driving prediction techniques for predictive energymanagement of plug-in hybrid electric vehicles," *J. Power Sources*, vol. 412, no. October 2018, pp. 480–495, 2019.

[2] European Commission, "Roadmap 2050 - Technical & Economic Analysis - Full Report," *Publications Office of the European Union*, pp. 1–100, 2016.

[3] J. Li *et al.*, "Dual-loop Online Intelligent Programming for Driver-oriented Predict Energy Management of Plug-in Hybrid Electric Vehicles," *Appl. Energy*, vol. 253, no. 2019, 2019.

[4] R. Bellman, "Dynamic Programming," *Science (80-.).*, vol. 153, no. 3731, pp. 34–37, 1966.

[5] A. Biswas and A. Emadi, "Energy Management Systems for Electrified Powertrains: State-of-The-Art Review and Future Trends," *IEEE Trans. Veh. Technol.*, vol. 68, no. 7, pp. 1–1, 2019.

[6] S. Il Jeon, S. T. Jo, Y. Il Park, and J. M. Lee, "Multi-mode driving control of a parallel hybrid electric vehicle using driving pattern recognition," *J. Dyn. Syst. Meas. Control. Trans. ASME*, vol. 124, no. 1, pp. 141–149, 2002.

[7] A. M. Phillips, M. Jankovic, and K. E. Bailey, "Vehicle system controller design for a hybrid electric vehicle," *IEEE Conf. Control Appl. - Proc.*, vol. 1, pp. 297–302, 2000.

[8] W. Enang and C. Bannister, "Modelling and control of hybrid electric vehicles (A comprehensive review)," *Renewable and Sustainable Energy Reviews*, vol. 74. pp. 1210–1239, 2017.

[9] Y. Huang, H. Wang, A. Khajepour, H. He, and J. Ji, "Model predictive control power management strategies for HEVs: A review," *J. Power Sources*, vol. 341, pp. 91–106, 2017.

[10] G. Paganelli, S. Delprat, T. M. Guerra, J. Rimaux, and J. J. Santin, "Equivalent consumption minimization strategy for parallel hybrid powertrains," *IEEE Veh. Technol. Conf.*, vol. 4, no. May 2014, pp. 2076–2081, 2002.

[11] C. Sun, F. Sun, and H. He, "Investigating adaptive-ECMS with velocity forecast ability for hybrid electric vehicles," *Appl. Energy*, vol. 185, pp. 1644–1653, 2017.

[12] M. Montazeri-Gh, A. Poursamad, and B. Ghalichi, "Application of genetic algorithm for optimization of control strategy in parallel hybrid electric vehicles," *J. Franklin Inst.*, vol. 343, no. 4–5, pp. 420–435, Jul. 2006.

[13] Q. Zhou *et al.*, "Modified Particle Swarm Optimization with Chaotic Attraction Strategy for Modular Design of Hybrid Powertrains," *IEEE Trans. Transp. Electrif.*, vol. 7782, no. c, 2020.

[14] Q. Zhou *et al.*, "Transferable representation modelling for real-time energy management of the plug-in hybrid vehicle based on k-fold fuzzy learning and Gaussian process regression," *Appl. Energy*, vol. 305, p. 117853, 2022.

[15] H. Ma, Z. Li, M. Tayarani, G. Lu, H. Xu, and X. Yao, "Computational Intelligence Non-model-based Calibration Approach for Internal Combustion Engines," *J. Dyn. Syst. Meas. Control*, vol. 140, no. April, pp. 1–9, 2017.

[16] Q. Zhou *et al.*, "Multi-step reinforcement learning for model-free predictive energy management of an electri fi ed o ff -highway vehicle," vol. 255, no. June, 2019.

[17] B. Shuai *et al.*, "Heuristic action execution for energy efficient charge-sustaining control of connected hybrid vehicles with model-free double Q-learning," *Appl. Energy*, vol. 267, 2020.

[18] F. Tao and Q. Qi, "Make more digital twins," *Nature*, vol. 573, no. 7775, pp. 490–491, 2019.

[19] Y. Lu, C. Liu, K. I. K. Wang, H. Huang, and X. Xu, "Digital Twin-driven smart manufacturing: Connotation, reference model, applications and research issues," *Robot. Comput. Integr. Manuf.*, vol. 61, no. July 2019, p. 101837, 2020.

[20] Q. Zhou *et al.*, "Transferable Representation Modelling for Real-time Energy Management of the Plug-in Hybrid Vehicle based on K-fold Fuzzy Learning and Gaussian Process Regression," *Appl. Energy*, 2021.

[21] F. Tao, H. Zhang, A. Liu, and A. Y. C. Nee, "Digital Twin in Industry: State-of-the-Art," *IEEE Trans. Ind. Informatics*, vol. 15, no. 4, pp. 2405–2415, 2019.

[22] J. Li, Q. Zhou, H. Williams, and H. Xu, "Digital Twin assisted Parallel Learning for Fuzzy Logic based Engine-powered Hybrid Propulsion Control System," in *International Conference on Advanced Vehicle Powertrains*, 2021.

[23] Ricardo, "Digital Engineering," 2021. .

[24] Q. Zhou, D. Zhao, B. Shuai, Y. Li, H. Williams, and H. Xu, "Knowledge Implementation and Transfer With an Adaptive Learning Network for Real-Time Power Management of the Plug-in Hybrid Vehicle," *IEEE Trans. Neural Networks Learn. Syst.*, pp. 1–11, 2021.

[25] Q. Qi and F. Tao, "Digital Twin and Big Data Towards Smart Manufacturing and Industry 4.0: 360 Degree Comparison," *IEEE Access*, vol. 6, pp. 3585–3593, 2018.

[26] M. Ehsani, Y. Gao, S. Longo, and K. Ebrahimi, *Modern electric, hybrid electric, and fuel cell vehicles*. CRC press, 2018.

[27] J. Li, Q. Zhou, Y. He, H. Williams, and H. Xu, "Driver-identified Supervisory Control System of Hybrid Electric Vehicles based on Spectrum-guided Fuzzy Feature Extraction," *IEEE Trans. Fuzzy Syst.*, vol. 6706, no. c, pp. 1–1, 2020.

[28] J. Li, Q. Zhou, H. Williams, and H. Xu, "Back-to-back competitive learning mechanism for fuzzy logic based supervisory control system of hybrid electric vehicles," *IEEE Trans. Ind. Electron.*, vol. 67, no. 10, pp. 8900–8909, 2020.

[29] J. Peng, H. He, and R. Xiong, "Rule based energy management strategy for a series–parallel plug-in hybrid electric bus optimized by dynamic programming," *Appl. Energy*, vol. 185, pp. 1633–1643, Jan. 2017.

[30] Z. Chen, R. Xiong, C. Wang, and J. Cao, "An on-line predictive energy management strategy for plug-in hybrid electric vehicles to counter the uncertain prediction of the driving cycle," *Appl. Energy*, vol. 185, pp. 1663–1672, 2017.
[31] J. Da Wu, C. C. Hsu, and H. C. Chen, "An expert system of price forecasting for used cars using adaptive neuro-fuzzy inference," *Expert Syst. Appl.*, vol. 36, no. 4, pp. 7809–7817, 2009.
[32] Y. Fu, Z. Gao, Y. Liu, A. Zhang, and X. Yin, "Actuator and sensor fault classification for wind turbine systems based on fast fourier transform and uncorrelated multi-linear principal component analysis techniques," *Processes*, vol. 8, no. 9, 2020.
[33] S. April, *Density Estimation for Statistics and Data Analysis*, no. 26. 1986.
[34] P. Rakshit and A. Konar, "Differential evolution for noisy multiobjective optimization," *Artif. Intell.*, vol. 227, pp. 165–189, 2015.
[35] H. Ma *et al.*, "Model-based Multi-objective Evolutionary Algorithm Optimization for HCCI Engines," *IEEE Trans. Veh. Technol.*, vol. 9545, no. c, pp. 1–1, 2014.
[36] K. Deb and J. Wiley, *Multi-objective optimization using evolutionary algorithms*. John Wiley & Sons, 2001.
[37] Y. He *et al.*, "Multiobjective component sizing of a hybrid ethanol-electric vehicle propulsion system," *Appl. Energy*, vol. 266, no. March, 2020.
[38] E. Zitzler, M. Laumanns, and L. Thiele, "SPEA2: Improving the strength Pareto evolutionary algorithm," 2001.
[39] Student, "The Probable Error of a Mean," *Biometrika*, vol. 6, no. 1, pp. 1–25, 1908.
[40] C. Musardo, G. Rizzoni, Y. Guezennec, and B. Staccia, "A-ECMS: An adaptive algorithm for hybrid electric vehicle energy management," *Eur. J. Control*, vol. 11, no. 4–5, pp. 509–524, 2005.

Ji Li (M'19) awarded the Ph.D. degree in mechanical engineering from the University of Birmingham (UoB), U.K, in 2020. He is currently a Research Fellow and works on the Connected and Autonomous Systems for Electrified Vehicles at the Vehicle Technology Research Centre. His current research interests include computational intelligence, informatic fusion, data-driven modelling, man-machine system, and their applications on connected and autonomous vehicles.

Quan Zhou (M'17) received the Ph.D. degree in mechanical engineering from the University of Birmingham in 2019 that was distinguished by being the school's solo recipient of the University of Birmingham's Ratcliffe Prize of the year. He is currently a Research Fellow and leads the Connected and Autonomous Systems for Electrified Vehicles Research at University of Birmingham. His research interests include evolutionary computation, fuzzy logic, reinforcement learning, and their application in vehicular systems.

Huw Williams graduated from the University of Oxford with a mathematics degree and received the Ph.D. degree in theoretical mechanics at the University of East Anglia. He is an Honorary Professor of Energy and Automotive Engineering at the UoB, Birmingham, U.K.

He is a professional mathematician with excellent skills in Lean, Six Sigma, Engineering Physics and Statistics. Huw has over 20 years' experience in the automotive industry. He also developed statistical skills through TQM in the 1980's culminating in his accreditation as Ford's top-scoring Master Black Belt in 2005.

Hongming Xu received the Ph.D. degree in mechanical engineering from Imperial College London, London, U.K. He is a full Professor of Energy and Automotive Engineering at the University of Birmingham, Birmingham, U.K., and Head of Vehicle and Engine Technology Research Centre. He has six years of industrial experience with Jaguar Land Rover. He has authored and co-authored more than 400 journal and conference publications on advanced vehicle powertrain systems involving both experimental and modeling studies.

Changqing Du received the Ph.D. degree from the Wuhan University of Technology, in 2009. After graduating with the Ph.D. degree, he conducted postdoctoral studies at SAIC-GM-Wuling Automotive Company, Ltd., from 2011 to 2013. From 2015 to 2016, he continued to visit The Ohio State University Automotive Research Center, as a Visiting Scholar. He is currently a Professor with the School of Automotive Engineering, Wuhan University of Technology. He is engaged in the research of new energy vehicles and their power plants.